Proceedings of the ASME 2016 International Mechanical Engineering Congress and Exposition
IMECE2016
November 11-17, 2016, Phoenix, Arizona, USA

IMECE2016-66164

UTILIZING REACTION WHEELS TO INCREASE MANEUVERABILITY AND LOCALIZATION ACCURACY OF A HOVERING ROBOT

Akin Tatoglu
Mechanical Engineering
University of Hartford
West Hartford, CT 06117 , USA
tatoglu@hartford.edu

Sean Greenhalge
Mechanical Engineering
University of Hartford
West Hartford, CT 06117 , USA
sgreenhalge@gmail.com

Kevin Windheuser
Mechanical Engineering
University of Hartford
West Hartford, CT 06117 , USA
k.windheuser@comcast.net

ABSTRACT

Hovercraft like vehicles have various advantages including traveling over almost any non-porous surface. Hovering bodies could use its thrusters to generate an active braking system. However, time required to stop and change direction of the propellers is not sufficient enough for sudden brake needs specifically in obstacle rich co-robot environment. Moreover, high speed sharp turn ability increases path planning algorithms efficiency by reducing overall mission time for any given simple task such as docking to power stations or more sophisticated tasks of sweeping unexplored areas. This paper discusses and examines the application of a reaction wheel mounted to a hovering body to allow for rapid maneuver. Reaction wheel is designed to have enough mass to adjust motion of the hovering robot due to unexpected drift or requested maneuver. Wheel would accelerate to high velocity and experience an instantaneous brake which allows energy stored in moment of inertia to be transferred from wheel to body. Detailed design approach, assembly steps, equations of motion and simulation results incorporated with generated path are discussed. Finally, set of real world experiments were executed and comparison plots are listed. Results showed that solution improves maneuverability of such structure substantially.

INTRODUCTION

Over the past years, the interest for the design of autonomous vehicles increases significantly. Various ground vehicle design and control approaches have been studied for multi terrain types including indoor and outdoor areas [1-2].

Hovercraft like vehicles have various advantages including traveling over almost any non-porous surface such as even or uneven terrain, sandy and icy grounds as well as water surface and could safely carry out transportation or exploration tasks [3]. Typically small hovercraft are good fit to be utilized as co-robots since they are close to the ground and travel at low speeds: failure or collisions do not cause serious damage [4].

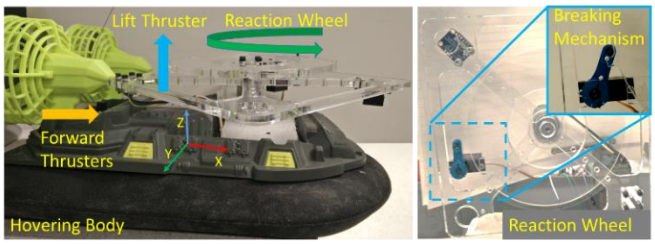

Fig.1 Hovering mobile body and reaction wheel

In this research paper we share our efforts on improving maneuverability of scaled indoor hovering exploration robot with a lift propeller and two differential drive propellers. In order to reach a stable and precise control of such structure, it is required to address maneuverability issues such as sudden stop requirements as well as lateral motion generation capabilities. For this purposes a reaction wheel [5] is manufactured and assembled onto an off the shelf hovering body as shown in Fig. 1 which is discussed in Sections-II.

Previous Work

Hovering bodies could use its thrusters to generate an active braking system. However, time required to stop and change direction of the propellers is not sufficient enough for sudden brake needs specifically in obstacle rich environments.

Moreover, lateral movement and high speed sharp turn ability increase path planning algorithms efficiency by reducing overall mission time for any given simple task such as docking to power stations or more sophisticated tasks of sweeping an unexplored area.

There have been several experiments utilizing autonomous or robotic hovercraft that have been previously performed [4, 6]. Hovering bodies provide excellent opportunities in testing a system that require a complex control scheme for stabilization and dynamics, while having a low chance of damage should the system fail. Such systems require a closed loop control scheme just to hold position steady due to the fact they rest on an essentially frictionless surface. Typically small hovercraft are close to the ground and travel at low speeds, so failure or collisions do not cause serious damage.

Larger autonomous vehicles can use sophisticated technology such as radar or GPS for localization [6], but for a smaller indoor vehicle Inertial Measurement Units (IMUs) might be more suitable. Visual sensors for localization purposes is another suitable solution. One such example is visual autocorrelation as inspired by insects such as flies or bees [6]. This method uses a small amount of visual sensors to find optic flow estimation, which is the rate of visual motion in radians per second.

For any given mission, robot will need to generate and execute a planned path which also requires motion planning to actuate necessary mechanisms. Planning logic is processed via multi-order algorithms, which create differential equations to define the curvature and frequencies of the path [9].

Specifically for co-robot systems its being collision free is vital. Real time motion planning is the combination of path planning— which relies on actuator constraints and dynamics of both the system and the environment— and obstacle avoidance. One approach to dynamic motion planning is that a robot moving through space essentially solves a static problem at successive intervals. However, each component of the problem, path planning and velocity planning, can be solved separately; the path among the obstacles is first selected, then the velocity is calculated along a path that best avoids the obstacles. Acceleration constraints as well as a minimum required time constraint must also be considered. The algorithm will calculate a velocity change in order to avoid collision with a moving object that may cross its path. If that is insufficient, a change in trajectory is also possible. Trajectory changes are also necessary for stationary objects [7-8].

Many algorithms rely on "configuration space". The configuration of a robot is its position in reference to an inertial frame. The configuration space is the set of all possible configurations. The collision free paths are the selected from the possible configurations, and the best path is selected from those options. If no configuration leads to collision free navigation the motion planning algorithm should terminate [7].

System constraints –such as system maneuverability— is key component determines path planning algorithm complexity. The error within the path following algorithm could be decreased using higher order algorithms [9-11]. However, mobile systems have limited power sources and higher order algorithms require exceedingly long time of processing and makes them less effective due to limited mobile processing power. On the other hand, increasing maneuverability could be advantageous to minimize calculation time and power consumption.

Reaction and momentum wheels had been utilized for various purposes including satellite position control to self-assembling swarm robotics [12-14]. A reaction wheel and momentum wheel are typically the same flywheel; however, their purpose might be different. A reaction wheel could transfer momenta stored in the rotating disc to the connected body by varying angular velocity such as rapid stops. Multi degree control could be executed by rotating the wheel in the opposite directions. On the other hand, continuously rotating momentum wheel increases the carries body's positional stability by resisting changes in moments. Good examples utilizing reaction wheels [14-15] study control of a cube shaped body with reaction wheels as well as self-assembling swarm robots. Design for both systems allows for precise movement with three flywheels, one per axis.

Our Approach

This paper discusses and examines the application of a reaction wheel mounted to a hovering mobile robot to allow for an immediate stop or maneuver. The reaction wheel is designed to have enough mass to adjust the motion of the hovering body due to unexpected drift or requested stop. The wheel would accelerate to a high velocity and experience an instantaneous brake which allows energy stored in moment of inertia to be transferred from wheel to hovering body.

Initially a standalone single degree-of-freedom flywheel system is studied: equations of motions are generated, system is simulated with varying wheel radiuses, wheel to body mass ratios as well as motor torque requirements and varying PID controller parameters are experimented to analyze response time, overshoot amplitudes and frequency responses. The transfer function is described with an input of applied torque to reaction wheel and outputs of angular position and forward velocity of the overall body. Analysis results were used to define appropriate motor requirements and design constraints.

The parts of the system, the body and the reaction wheels are built utilizing laser CNC machined parts and plates. Prior to design and material selection process, a stress analysis is adopted to test whether or not the material for the reaction wheel will be able to withstand the impact of the braking mechanism stopping it.

The mass of the body and wheel was set at a high ratio; however, depending on the applications and materials used these figures can be adjusted accordingly. As the wheel loses weight, the energy has to be compensated with increased angular velocity of the wheel. Friction values are empirically calculated as parts were chosen. Finally, initial system simulation results and experimental comparisons plots are listed. Also, overall system capability is benchmarked by comparing generated trajectories with and without reaction wheels. It is shown that high velocity turn radius is minimized and system has a higher localization accuracy while following pre-defined trajectory.

Next section discusses the mathematical equations and simulation results of individual reaction wheel followed by manufacturing and control structure of the system. Finally experimental setup is described and real world experiment results are listed before the conclusion and future work section.

NOMENCLATURE

θ_b, θ_f	Angular position of body and flywheel
l_b,l_f	Length from the pivot point
m_b,m_f	Mass of the body and flywheel
I_b , I_f	Moment of inertia of the body and flywheel
τ	Torque generated by motor
M_H, M_f	Moments of hovering robot and flywheel
k_f	Stiffness of the shaft
r_c	Capture radius

REACTION WHEEL DESIGN AND DEVELOPMENT

Equation of Motion

With θ_b as the angular position of the body, and θ_f as the angular position of the flywheel with respect to the body, equations of motion are given by

$$\ddot{\theta}_b = \frac{(m_b l_b + m_f l_f) * g * \sin(\theta_b) - \tau - f_b \dot{\theta}_b + f_f \dot{\theta}_f}{I_b + m_f {l_f}^2} \quad (1)$$

$$\ddot{\theta}_f = \frac{(I_b + I_f + m_f {l_f}^2) * (\tau - f_f \dot{\theta}_f)}{I_f * (I_b + m_f {l_f}^2)} - \frac{(m_b l_b + m_f l_f) * g * \sin(\theta_b) - f_b \dot{\theta}_b}{I_b + m_f {l_f}^2} \quad (2)$$

where m_b is the mass of the body, including any mass attached, such as the braking system. m_f and I_b represent the mass of the flywheel and moment of inertia of the body around the pivot point respectively. I_f is the moment of inertia of the flywheel around the axis of the motor. The lengths $l_b$and l_f represent the length from the pivot point to the center of mass of the body and the pivot point to the center of mass of the wheel, respectively. τ is the torque of the motor. Dynamic friction coefficients of the system are represented by f_b – friction where the body is mounted— and f_f , friction of the motor when it is not being torqued.

In the equation of motion for the body, the first term "$(m_b l_b + m_f l_f) * g * \sin(\theta_b)$" represents the torque created by both the body and the wheel due to gravity. They are essentially acting as an inverted pendulum, pulling the body downwards away from the vertical axis. The terms "$f_b \dot{\theta}_b$" and "$f_f \dot{\theta}_f$" are the impact of the friction as a result of the rotational speed of the body and flywheel respectively. The denominator represents the sum inertia of the system with respect to the pivot point, at one corner of the body.

The equation of motion for the flywheel has been simplified so that a term could be created that was very similar to the equation of motion for the body. This shows that the flywheel's acceleration is directly influenced by the motion of the body.

Block Diagram

The equations of motion representing mechanical illustration are used to design the block diagram. Followed steps are as following: Each equation is represented as a summing junction of all its terms. The output of the summing junctions can be integrated to get $\dot{\theta}$ and θ, which are then multiplied by constants and entered into the summing junctions that represent the equation. Final block diagram with feedback loops is presented in Fig. 2.

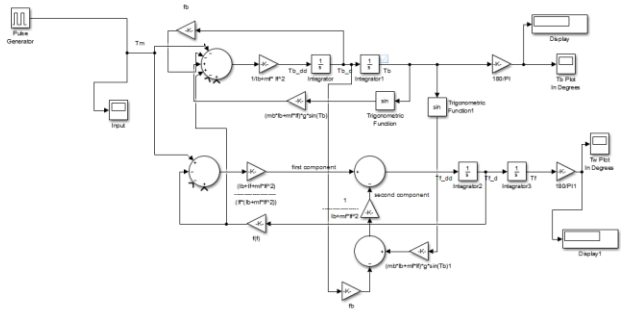

Fig.2 Block diagram of individual reaction wheel

The input of the control system is torque supplied by motor and input signal is simulated by a pulse generator to study behavior of the system and plots are shown in Fig. 3.

Fig. 3: Input signal impulses are sent at controlled intervals.

Multiple pulse generators are used to send pulses in opposite directions at regular intervals. This allows the body to be knocked in multiple directions. Each gain block, marked with {k} is determined by plugging empirical values generated in initial experiments. The terms Tf_{dd} and Tb_{dd} represent $\ddot{\theta}_f$ and $\ddot{\theta}_b$ respectively, which are then integrated twice to give the outputs of the positional location of both the flywheel and the body in radians. Finally, values are converted to degrees and plot is shown in Fig. 4. This allows the input to be varied to ensure that the system behaves as expected.

Simulation Results

Several basic tests were run to ensure the system behaves as expected. Different pulses are run as the input to see how the system reacts. The system starts at θ_b equal to zero degrees, which is vertical. A pulse of the motor is sent, which knocks the system off axis, which then swings around until it is at 180 degrees, as shown in Fig. 4, where it eventually comes to a rest.

The values for the friction coefficient and mass values are changed to determine system reaction.

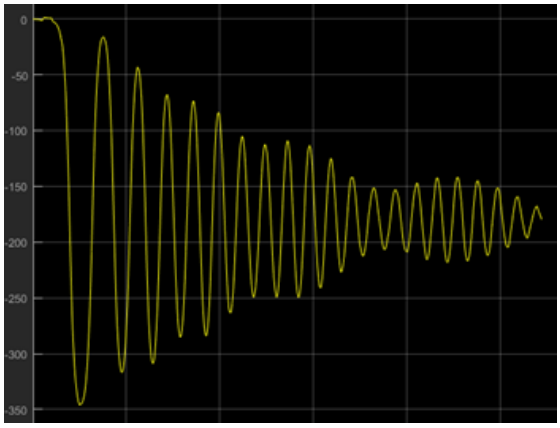

Fig 4. Response of reaction wheel. The body swings and comes to a rest near -180˚

After initial simulations, multiple pulses are supplied to the block diagram methodologically to identify boundaries which bounces the body back and forth about the vertical axis. Findings had showed that angular position of the body can be controlled just by a sudden acceleration or deceleration of the flywheel.

Design Process and Development

Prior to designing the momentum wheel, application requirements were studied. First challenge was to design a structure to brake a momentum wheel rapidly. Multi teeth structure at outer edge of the momentum wheel was chosen to implement design. These teeth components acts as a barrier and collide into servo motor controlled braking arm mechanism as shown in Fig. 5 and the wheel design as in Fig. 6.


Fig.5 Braking mechanism acting on tooth barrier

Design iterations of momentum wheels are presented at Fig. 7 (a) and (b). After various tests with initial design (Fig. 7-a), it was observed that barriers did not latch on to the brake fast enough to allow for optimal energy transfer from rotating to stationary bodies. The second design iteration (Fig. 7-b) is incorporated a “T” shaped teeth design that guarantees braking mechanism to be hooked and reach to a full stop rapidly which efficiently transfers energy.

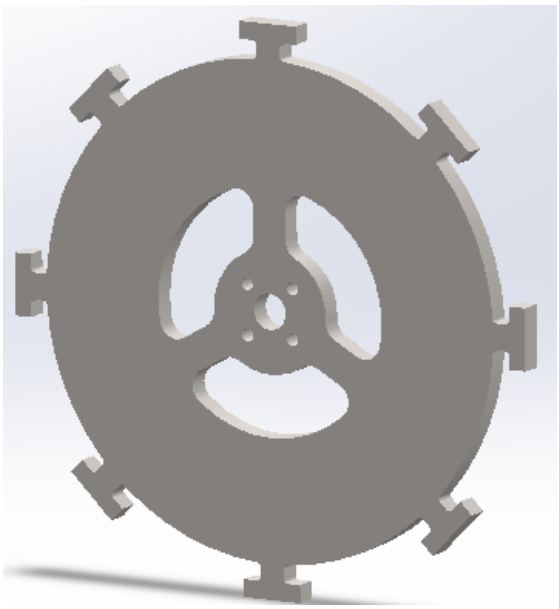
Fig.6 SolidWorks Wheel Design

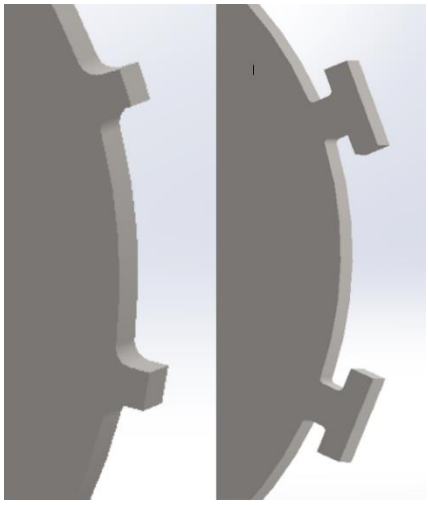
Fig.7 Momentum wheel collision teeth design. a) Left: Initial design b) Right: Next design with T shaped structure

During material selection process weight, strength and machining options were investigated. Extruded acrylic Plexiglas was chosen to manufacture the body. After required weight calculations, thickness was set to ¼ inch +/- 0.015. For accurate dimensioning material is cut with a laser CNC.

The weight of momentum wheel was critical as the weight had to be large enough to overcome the friction and other forces acting on the hovercraft. Calculated by the initial simulations discussed in previous paragraphs, it was determined that the ideal weight ratio between body and wheel would be 2:1. After initial experiments, weight is calibrated by adding five 20 gr. masses. Final mass ratio of wheel body to overall system is 7:1 where total mass is 1452 gr.

CONTROL STRUCTURE AND DEVELOPMENT OF MOBILE HOVERING ROBOT

Overall System Model

System is modeled with a simplified unrestrained two disk structure. While top disk represents the reaction wheel, bottom disk represents both wheel body and hovering robot whose inertia I_H is simplified to a single mass as shown in

$$\begin{bmatrix} I_f & 0 \\ 0 & I_H \end{bmatrix} \begin{bmatrix} \ddot{\theta}_f \\ \ddot{\theta}_H \end{bmatrix} + \begin{bmatrix} k_f & -k_f \\ -k_f & k_f \end{bmatrix} \begin{bmatrix} \theta_f \\ \theta_H \end{bmatrix} = \begin{bmatrix} M_f \\ M_H \end{bmatrix} \quad (3)$$

where subscript {H} represents the hovering body. Stiffness of shaft is represented by k_f and momenta's on flywheel and hovering body are represented by M_f and M_H. For simplicity, shape of hovering body is assumed to be a rectangular parallelepiped for moment of inertia calculations and air friction is ignored.

Simulation Results

Overall system with and without reaction wheel is simulated. First a path with waypoints is defined. Then model of the system is simulated without reaction wheel to generate a motion plan as shown in Fig. 8.

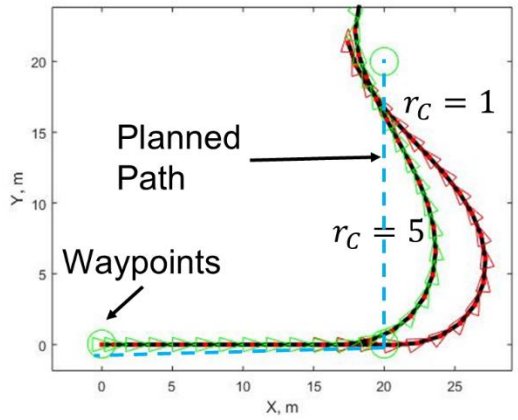

Fig. 8 Trajectory simulation of motion plan with different capture radii, without reaction wheel. (r_c: Capture radius)

Green circles represent waypoints and blue dashed line is the expected trajectory with zero error. However, turn which is defined to be 90º is challenging and requires a full stop to execute the motion with zero path following error. Another challenge is to reach a full stop in short amount of time since friction is little. To avoid such delay, a capture radius is defined that robot will attempt to initialize a turn prior to reaching to corner. Two trajectories are generated using capture radius (r_C) of 1 and 5 units. It is clearly shown that higher r_C reduced the overall error. Even in this case, generated trajectory is still ~4 units off from the waypoint.

Another simulation is executed to compare the effect of the reaction wheel for the same scenario. In Fig. 9 three trajectories are presented. Green plot represents a trajectory without reaction wheel and used for comparison purposes. Blue and red curves are executed while reaction wheel is active. As discussed, lower capture radius might increase error. However, with a reaction wheel –even with capture radius of 3 or even 1— local and overall path following error is substantially reduced. The results and error amounts could be clearly observed at Fig. 9. Moreover, time required to execute a turn is reduced, too. These simulation results were used to design the real world experiments.

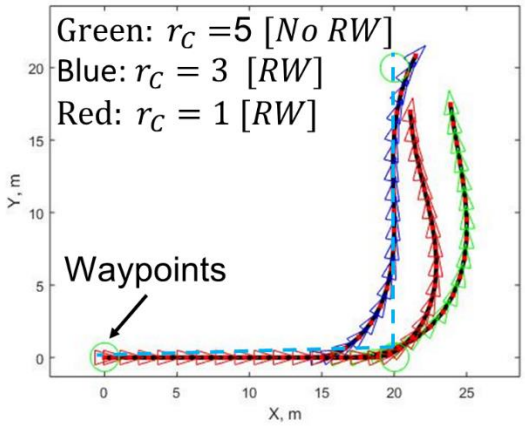

Fig. 9 Trajectory simulation of motion plan execution comparison with and without reaction wheel (RW) and with different capture radii. (r_c: Capture radius)

EXPERIMENTAL DESIGN

System Assembly

Steps of assembling the wheel to the hovering body included redesigning off-the-shelf system's power supply, designing a support for the momentum wheel as well as braking mechanism and assembly of electrical and microprocessor components. Final design was a mobile system controlled with an Arduino board with shields powered by two high discharge batteries as presented in Fig. 10. During these steps, key challenge was even weight distribution of individual components while keeping air flow channels open since even small eccentric caused system drift unintentionally.

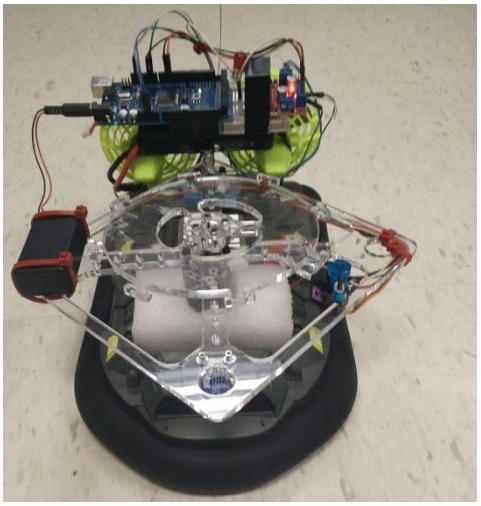

Fig. 10 Hovercraft with internally powered and controlled momentum wheel

Design of the bracket which was bolted to the body is shown at Fig. 11. This bracket was made out of the same material as the reaction wheel and was machined with laser CNC as well. Foam was used to support the motor in the bay to reduce vibration. System is powered with two 12 volts high discharge batteries.

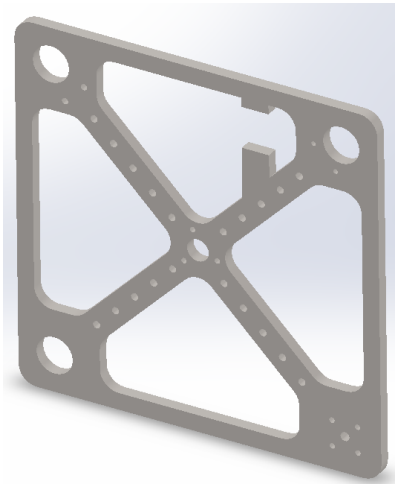

Fig. 11 SolidWorks drawing of bracket

An Arduino board is used to execute various motion profiles. This microcontroller was chosen for its rapid prototyping capabilities, low power consumption and low weight. For image processing purposes two status indicator LED's were attached to the body. Connection diagram details are presented in Fig. 12. A metal gear servo motor is used to trigger braking mechanism. Reaction wheel motor torque is controlled with an L298N Dual H-Bridge chip. The microcontroller and motor controller were mounted on top of the battery.

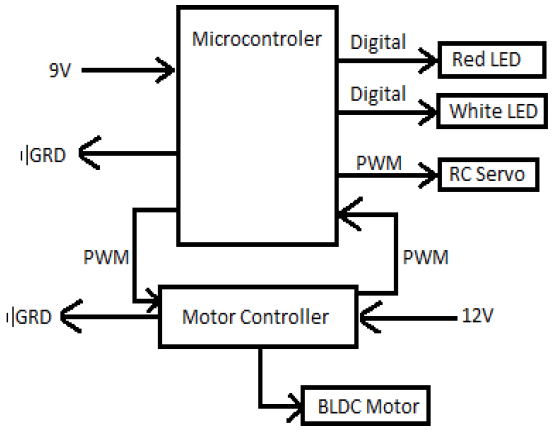

Fig. 12 Schematic diagram of the electronics setup

Experimental Setup

As discussed in previous sections, various experiments were executed to analyze the behavior of capture radius and empirically plot the trajectory of the hovering robot. Table 1 lists the experiments.

Table 1. List of experiments executed

	1	2	3	4
A	**STRAIGHT LINE, NO REACTION WHEEL**			
1	STOP[1s]	STOP[1s]	STOP[1s]	STOP[1s]
2	FORWARD [1 s]	FORWARD [2 s]	FORWARD [3 s]	FORWARD [4 s]
3	STOP[1s]	STOP[1s]	STOP[1s]	STOP[1s]
B	**STRAIGHT LINE, REACTION WHEEL IS ACTIVE**			
	START WHEEL	START WHEEL	START WHEEL	START WHEEL
1	STOP[1s]	STOP[1s]	STOP[1s]	STOP[1s]
2	FORWARD [1 s]	FORWARD [2 s]	FORWARD [3 s]	FORWARD [4 s]
3	STOP WHEEL [in 1 s]	STOP WHEEL [in 1 s]	STOP WHEEL [in 1 s]	STOP WHEEL [in 1 s]
4	STOP[1s]	STOP[1s]	STOP[1s]	STOP[1s]
C	**TURN, NO REACTION WHEEL**			
1	STOP[1s]	STOP[1s]	STOP[1s]	STOP[1s]
2	FORWARD [2 s]	FORWARD [2 s]	FORWARD [2 s]	FORWARD [2 s]
3	TURN LEFT [0.5 s]	TURN LEFT [0.5 s]	TURN LEFT [0.5 s]	TURN LEFT [0.5 s]
4	FORWARD [2 s]	FORWARD [2 s]	FORWARD [2 s]	FORWARD [2 s]
5	STOP[1s]	STOP[1s]	STOP[1s]	STOP[1s]
D	**TURN, REACTION WHEEL IS ACTIVE**			
	START WHEEL	START WHEEL	START WHEEL	START WHEEL
1	STOP[1s]	STOP[1s]	STOP[1s]	STOP[1s]
2	FORWARD [2 s]	FORWARD [2 s]	FORWARD [2 s]	FORWARD [2 s]
3	TURN LEFT [0.5 s]	TURN LEFT [0.5 s]	TURN LEFT [0.5 s]	TURN LEFT [0.5 s]
4	FORWARD [2 s]	FORWARD [2 s]	FORWARD [2 s]	FORWARD [2 s]
5	STOP[1s]	STOP[1s]	STOP[1s]	STOP[1s]

First of all, to log acceleration and deceleration values of the body without reaction wheel, a straight line experiment is executed (Table 1, A and B). Same experiment is repeated with different time intervals of motion (forward thrust from propellers) as well as with reaction wheels. After then, turn capabilities of the system is investigated, again, with and without the reaction wheel (Table 1, C and D). Results are discussed in the following section.

For measurement purposes a top view camera is used and ground is marked with equally spaced markers. Fig. 11 presents top view camera tripod location and a superimposed image of the hovering robot.

Fig. 11 Left: Example experimental scene. Right: Superimposed image from top view camera

EXPERIMENTAL RESULTS

Initial Drift Behavior

As discussed in Section-1, rotating mass mounted on a body increases the resistance of a system –while in equilibrium— to external forces. Fig. 13 shows a typical result from experiments with and without reaction wheel: When the system initially hovers itself, specifically on non-flat surfaces, a random change in heading is observed in most cases. However, when same action is executed while reaction wheel is active, initial unintended drift is minimized. Therefore, most suitable sequence of action is to initiate reaction wheel first, when the body is contacting with the ground that unexpected change of heading is avoided. Moreover, initial angular acceleration of the wheel (while wheel is reaching from zero to constant angular velocity) will not cause an unintended change and initial drift caused by uneven surface and uneven system dynamics are minimized since mechanism is acting as a momentum wheel that reduces sensitivity of heading to surface angle.

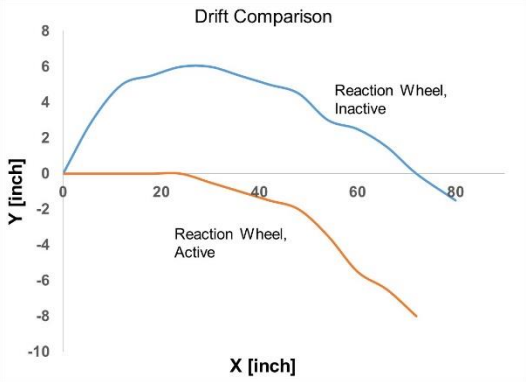

Fig. 13 Trajectory plot. Initial drift is minimized with reaction wheel

Displacement occurs on individual axes is presented in Fig. 14. It is clearly shown that both X and Y had displaced more when reaction wheel is active. Main reason of this type of behavior is that heading was already adjusted by the wheel in earlier stage of robot's motion. Moreover, in the same amount of time, heading angle displaced double the amount compared to the value without wheel which is discussed in the following figure.

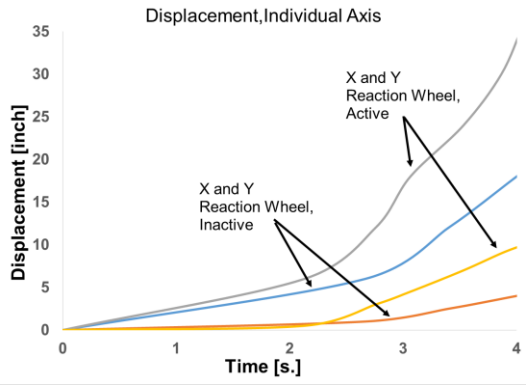

Fig. 14 Individual axis displacement with and without wheel

Angular displacement comparison is shown in Fig. 15. The beginning of the motion is more stable as discussed in the previous subsection. Initial angular change of the blue curve, is an unintended drift: prior to rotation command is sent to the robot. After command is sent, the curve with reaction wheel acts twice faster that it minimizes capture radius requirement as discussed in the simulation results of previous section. It is clear that system has a rapid maneuverability while reaction wheel is active.

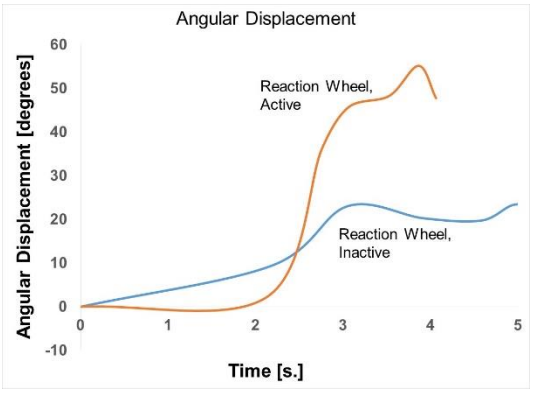

Fig. 15 Angular displacement with and without wheel

CONCLUSIONS AND FUTURE WORK

We have shared our efforts to design, develop and control a path following hovering robot with a reaction wheel mounted on top. Main goal of this research project is to increase the maneuverability of hovering body that it could be safely used as a co-robot and for other tasks such as multi-terrain exploration and transportation.

First equation of motions of an individual reaction wheel was derived and they were studied with simulations. By using initial outcomes, an iterative mechanical design approach is applied to address each challenge one at a time. Finally, system is built and tested.

Various motion profiles were simulated in virtual environment to identify ideal capture radius for sharp turns of such vehicle. Then, similar motion plans were executed with real world experiments. Results are compared and it is shown not only in simulation but also in real world experiments that even capture radius is reduced, system trajectory generates less displacement error. Moreover, initial drift is minimized and total path following error is substantially reduced. While solution increases computational complexity of the system, we have shown that our novel solution could increase controllability and maneuverability of hovering mobile robots and vehicles.

In the following steps of our research, redundancy and stability of system in maze like environment will be tested. In addition to that, it will be compared with wheeled structures to investigate the advantages and disadvantages of proposed solution.

ACKNOWLEDGMENTS

We would like to thank to Claudio Campana, Dr. Robert Celmer, Dr. Eoin King, Phil Faraci, Rebeccah Tuscano-Moss, Ray Miller, Toby Poole and Dr. Patricia Mellodge for their generous helps.

REFERENCES

[1] Stavens, D., and Thrun, S., 2006, "A Self-Supervised Terrain Roughness Estimator for Off-Road Autonomous Driving," Proc. Twenty-Second Conf. Annu. Conf. Uncertain. Artif. Intell., pp. 469–476.

[2] Biswas, J., and Veloso, M., 2012, "Depth camera based indoor mobile robot localization and navigation," IEEE Int. Conf. Robot. Autom., pp. 1697–1702.

[3] Miková, Tomáš Lipták–Alexander Gmiterko–Ľubica, Erik Prada. "Design of Mobile Robot Based on Hovercraft," CER Comparative European Research 2014 pp.101-104.

[4] Stubbs, A., Vladimerou, V., Fulford, A. T., King, D., Strick, J., and Dullerud, G. E., 2006, "Multivehicle systems control over networks: A hovercraft testbed for networked and decentralized control," IEEE Control Syst. Mag., **26**(3), pp. 56–69.

[5] Babuska, V., Beatty, S. M., Brett, J., and Fausz, J. L., 2004, "A Review of Technology Developments in Flywheel Attitude Control and Energy Transmission Systems," IEEE Aerosp. Conf., pp. 2784–2800.

[6] Fuller, S. B., and Murray, R. M., 2011, "A hovercraft robot that uses insect-inspired visual autocorrelation for motion control in a corridor," 2011 IEEE Int. Conf. Robot. Biomimetics, ROBIO 2011, pp. 1474–1481.

[7] Frazzoli, E., Dahleh, M. a, and Feron, E., 2002, "Real-time motion planning for agile autonomous vehicles," AIAA J. Guid. Control, **25**(1), pp. 116–129.

[8] Fiorini, P., and Shiller, Z., 1998, "Motion Planning in Dynamic Environments using Velocity Obstacles," I. J. Robot. Res, **17**, pp. 760–772.

[9] Gonzalez, C., and Schlegel, H. B., 1991, "Improved algorithms for reaction path following: Higher-order implicit algorithms," J Chem Phys, **95**(8), pp. 5853–5860.

[10] Samson, C., 1995, "Control of Chained Systems Application to Path Following and Time-Varying Point-Stabilization of Mobile Robots," IEEE Trans. Automat. Contr., **40**(1), pp. 64–77.

[11] Azinheira, J. R., de Paivab, E. C., Ramos, J. J. G., and Bueno, S. S., 2000, "Mission Path Following for an Autonomous Unmanned Airship," Proc. 2000 ICRA. Millenn. Conf. IEEE Int. Conf. Robot. Autom., (April), pp. 1269–1275.

[12] Chen, X., Steyn, W. H., Hodgart, S., and Hashida, Y., 1999, "Optimal Combined Reaction-Wheel Momentum Management for Earth-Pointing Satellites," J. Guid. Control. Dyn., **22**(4), pp. 543–550.

[13] Landis Markley, F., Reynolds, R. G., Liu, F. X., and Lebsock, K. L., 2010, "Maximum Torque and Momentum Envelopes for Reaction Wheel Arrays," 2Journal Guid. Control Dyn., **33**(5), pp. 1606–1614.

[14] Li, S., Katzschmann, R., and Rus, D., 2015, "A soft cube capable of controllable continuous jumping," pp. 1712–1717.

[15] Muehlebach, M., Mohanarajah, G., and D'Andrea, R., 2013, "Nonlinear analysis and control of a reaction wheel-based 3D inverted pendulum," Proc. IEEE Conf. Decis. Control, pp. 1283–1288.